Realizing Stable Zigzag Polymeric Nitrogen Chains in P-N Compounds

Chengfeng Zhang[1,2], Guo Chen[1,2], Yanfeng Zhang[1,3], Jie Zhang[1*], and Xianlong Wang[1,2*]

[1]*Key Laboratory of Materials Physics, Institute of Solid State Physics, HFIPS, Chinese Academy of Sciences, Hefei 230031, China*
[2]*University of Science and Technology of China, Hefei 230026, China*
[3]*Institutes of Physical Science and Information Technology, Anhui University, Hefei 230601, China*

(Received 2 December 2025; accepted manuscript online 2 February 2026)

The zigzag nitrogen chain, similar to the Ch-N structure, has long been considered as a potential high-energy-density structure. However, all the previously predicted zigzag N-chain structures, similar to Ch-N, exhibited imaginary frequencies in their phonon spectra at 0 GPa. Here, we conducted a systematic investigation of P-N compounds using first-principles calculations, uncovering a series of structurally similar stable phases, $C2/m$-PN_x (x = 6, 8, 10, 12, and 14), in which N forms zigzag N chains similar to those in Ch-N. In P-N compounds, the longest zigzag N-chain, which can theoretically remain stable under ambient pressure, is the N-chain composed of 14 N atoms in $C2/m$-PN_{14}. If the N-chain continues to grow, imaginary interchain vibrational frequencies arise in the system. Notably, N chains with an even number of atoms were more likely to be energetically favorable. The five $C2/m$-PN_x phases and one metastable phase (R-PN_6) exhibited remarkable stability and excellent detonability at ambient pressure, indicating that they are promising candidates for high-energy-density materials. In addition, R-PN_6 was the first structure to stabilize the N_6 ring through covalent bonding, with the covalent network contributing to its high hardness (47.59 GPa).

DOI: 10.1088/0256-307X/43/3/030801 CSTR: 32039.14.0256-307X.43.3.030801

1. Introduction. Polymeric N materials have garnered significant attention owing to their cleanliness and high energy density and have important potential applications as high-energy-density materials (HEDMs).[1,2] Theoretical studies have reported a variety of novel polymeric N structures, including typical molecular crystals like N_{16} and N_{10},[3,4] cage-like N_{10},[5] chain-like phases such as Ch-N and Cmcm-N,[6,7] layered structures such as BP, PP, LB, ZS, and A7 phase,[8–11] three-dimensional network such as cg-N and Pnnm phase.[12,13] In 2004, cg-N was successfully synthesized under extreme conditions of 2000 K and 110 GPa,[12] marking the first experimental synthesis of polymeric N structures predicted by theory. Subsequently, BP-N, LP-N, and HLP-N were successfully synthesized at the high pressures of 140, 150, and 250 GPa, respectively.[14–16] In addition to traditional high-pressure and high-temperature approaches, polymeric N has been successfully synthesized in recent years via plasma and chemical methods. These emerging avenues offer perspectives for the synthesis of polymeric N.[17–19]

N-rich materials doped with various elements have attracted considerable attention to obtain more polymeric N under mild conditions. Similar to pure N materials, N-rich compounds exhibit a variety of N configurations. As reported in theoretical studies, the configurations of N in these materials primarily include zero-dimensional ring structures,[20–22] one-dimensional chain structures,[23–28] two-dimensional layered structures,[29,30] and three-dimensional network structures.[31,32] In zero-dimensional ring structures, the N_5 ring tends to acquire electrons from impurity atoms, thus achieving good stability.[33] One-dimensional chain structures, on the other hand, generally require lower synthesis pressures.[34] As a result, many experimental synthesis of zero-dimensional[35–38] and one-dimensional structures[39–42] were reported. However, no zigzag nitrogen chain structure was observed in these experiments. This zigzag N-chain is believed to possess a wide variety of physical properties, including superconductivity and high energy density.[7] Therefore, searching a standard zigzag N-chain for N-rich systems is crucial. Previous research has indicated that the introduction of P into pure N materials can promote the polymerization of N.[43] Furthermore, the electronic structure of P is similar to that of N, and doping with P may successfully induce the zigzag N chains reported in pure N systems within N-rich systems. Therefore, we conducted an in-depth research on P-N compounds.

In this study, structural searches and first-principles calculations were conducted. $C2/m$-PN_x (x = 6, 8, 10, 12, and 14) containing zigzag N chains were discovered, and these structures were found to be dynamically stable under ambient pressure, exhibiting good detonation performance. The reason why infinitely long zigzag N chains, such as those in Ch-N structures, cannot be synthesized experimentally is explained. In addition, we discovered that R-PN_6 contains an N_6 ring, and this zero-dimensional cyclic structure stabilized by covalent bonds was reported

*Corresponding authors. Email: jzhang@theory.issp.ac.cn; xlwang@theory.issp.ac.cn
© 2026 Chinese Physical Society and IOP Publishing Ltd. All rights, including for text and data mining, AI training, and similar technologies, are reserved.

for the first time in N-rich compounds.

2. Methods. The structure prediction for the P-N system was performed using the particle swarm optimization methodology implemented in the CALYPSO code.[44] Structural searches were conducted on the PN_x (x = 3, 4, 5, 6, 7, 8, 10, 12, and 14) compounds across pressures ranging from 0 to 150 GPa with 1–3 formula units. First-principles calculations of the structural and electronic properties based on density functional theory utilizing a plane-wave basis set were performed using the Vienna ab initio simulation package.[45] The generalized gradient approximation (GGA)[46,47] parameterized by the Perdew (PBE)[48] exchange-correlation functional, along with the projected augmented wave (PAW)[49] was employed for the calculations. Computational accuracy was ensured with a grid density of 0.03 $Å^{-1}$ and an energy cutoff of 520 eV. The formation enthalpies ΔH_f of PN_x compounds are determined using the formula $\Delta H_f(PN_x) = [H(PN_x) - H(P) - xH(N)]/(1+x)$, where $H(PN_x)$ is the enthalpy of PN_x. $H(P)$ and $H(N)$ are the enthalpies of $Pm\bar{3}m$-P,[50] ε-N,[51] and cg-N, respectively.[12] The phonon dispersion relations were calculated using the Phonopy code based on the finite displacement method.[52] The PBE-vdW method was employed for all the structures.[53] Detonation velocity and pressure were derived using the Kalet–Jacobs equation,[54] and the crystal orbital Hamilton population (COHP) was calculated using the LOBSTER program.[55] The Bader charge of the structure was calculated using VTST.[56–59] Additionally, VASPKIT was adopted in our work.[60]

3. Results and Discussion. The convex-hull curve was constructed based on the formation enthalpies of the thermodynamically stable structures, and the convex-hull curves at different pressures are shown in Fig. 1(a) and Fig. S1. We found that at 0 GPa, only P_3N_5 was present on the convex hull, which is consistent with previous experimental observations and theoretical simulations.[61,62] With pressure increasing to 43 GPa, PN_6 with $C2/m$ symmetry become stable on the convex hull. Furthermore, we can observe that the other PN_x (x = 4, 8, 10, 12, and 14) with the same $C2/m$ symmetry are very close to the convex hull. For example, PN_8 and PN_{10} are only 27 and 65 meV/atom above the convex-hull curve, respectively. When the pressure was increased to 53 GPa, in addition to $C2/m$-PN_6, $C2/m$-PN_x (x = 8, 10, 12, and 14) became stable; the corresponding structures are shown in Figs. 2(a)–2(e). Recently, a theoretical structural search was applied to the compositions of PN_x (x = 2, 3, and 4), revealing that PN_4 became stable at a pressure of 50 GPa.[62] However, if components with higher N contents are included, the previously reported P2/m-PN_2, Immm-PN_3, and $C2/m$-PN_4 are located above the convex hull at 50 GPa. The $C2/m$-PN_6 continues to remain energetically favorable as the pressure reaches 100 GPa, where $C2/m$-PN_4 also reappears in our search. The stable pressure range of $C2/m$-PN_x is shown in Fig. 1(b), and $C2/m$-PN_6 exhibits the widest stable pressure range from 43 GPa to 100 GPa, indicating that $C2/m$-PN_6 possesses the highest stability among the N-rich phases in our predictions. $C2/m$-PN_8 becomes metastable at approximately 58 GPa, while $C2/m$-PN_{10} become metastable at around 55 GPa. Similarly, both $C2/m$-PN_{12} and $C2/m$-PN_{14} become metastable at approximately 58 GPa. Although the stable pressure range of $C2/m$-PN_x (x = 8, 10, 12, and 14) is relatively narrow, these structures resemble convex hulls over a broad pressure range of 50–100 GPa. Therefore, they are promising candidates for experimental observations under high pressure.

As shown in Figs. 2(a)–2(e), all of newly discovered N-rich phases, $C2/m$-PN_x (x = 6, 8, 10, 12, and 14), exhibit striking structure similarities, where N atoms forming zigzag chains. As the N content increases, the length of the zigzag N chains also increases. In these stable phases, the coordination number of P is six, and the six N atoms form an octahedron around the central P atom. The main difference between these phases is the number of N atoms

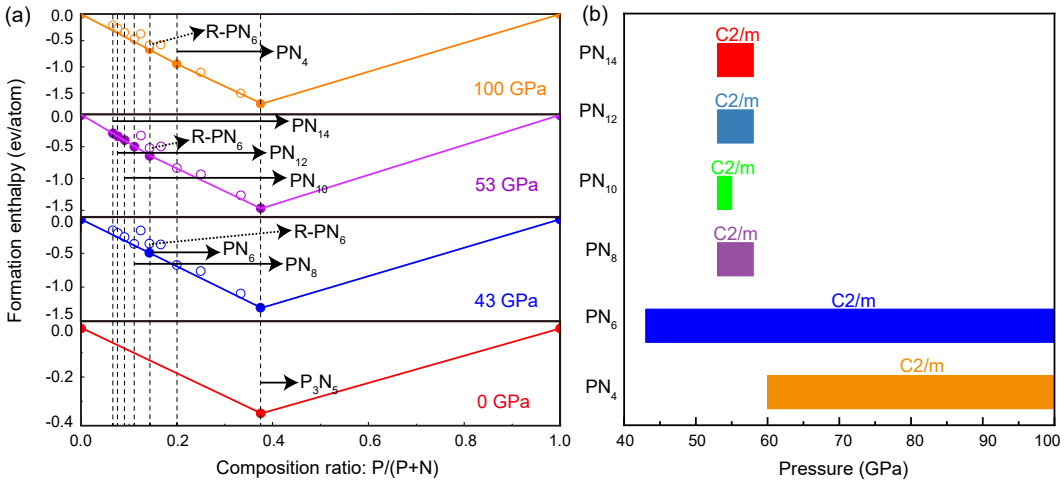

Fig. 1. Thermodynamic stability of P-N compounds. (a) Formation enthalpies of vaious PN_x (x = 2, 3, 4, 5, 6, 7, 8, 10, 12, and 14) compounds (with respect to pure P and pure N). Stable phases are represented by solid dots, while unstable/metastable phases are represented by hollow dots. The hollow circle corresponding to PN_6 is R-PN6, which is just located 66 meV/atom above the convex-hull curve at 100 GPa. (b) Pressure-composition phase diagram of the predicted P-N phases.

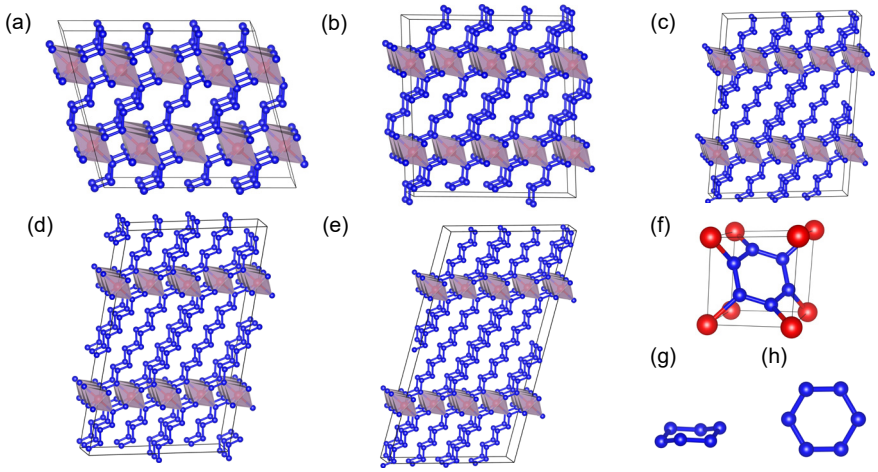

Fig. 2. Crystal structures of P-N compounds at 0 GPa. (a) $C2/m$-PN_6, (b) $C2/m$-PN_8, (c) $C2/m$-PN_{10}, (d) $C2/m$-PN_{12}, (e) $C2/m$-PN_{14}, (f) R-PN_6, (g) Side perspective of the N_6 ring in R-PN_6, (h) Top view of the N_6 ring in R-PN_6. Red represents P atoms, and blue represents N atoms.

within the chains. Furthermore, the local coordination environment of P in $C2/m$-PN_x (x = 6, 8, 10, 12, and 14) is consistent with that in P_3N_5 under high pressure, with a coordination number of six (see Fig. S2), whereas at low pressure, the coordination number of P in αP_3N_5 is four. This suggests that the formation of P-N octahedra in the P-N system under high pressure is favorable for the stability of the system. Under high pressure, as the N content increased, the P-N octahedra acted as a framework, stabilizing the zigzag N chains formed by the newly added N atoms. The structures of the previously reported PN_4 (Fig. S2) closely matched those of the $C2/m$-PN_x (x = 6, 8, 10, 12, and 14) series. This consistency suggests that the $C2/m$-PN_x structure is robust under high pressures. Additionally, $P\bar{3}1c$-PN_4 is an ultrahard material;[63] in this material, phosphorus is also six-coordinate, whereas the nitrogen atoms do not polymerize into chain-like structures. Overall, our structures possessed a higher nitrogen content, making them more suitable for HEDMs.

For R-PN_6, the space group was $R\bar{3}m$, and the coordination number of the P atoms was six. Unlike in $C2/m$-PN_x, N aggregation in R-PN_6 takes the form of a noncoplanar N_6 ring. Because of the small electronegativity difference between P and N, the six P atoms surrounding the N_6 ring form six covalent bonds with each N atom in the N_6 ring. These six covalent bonds collectively stabilized the central N_6 ring. In N-rich environments, N_6 rings are stabilized by ionic bonds with the dopant atoms.[21,64–66] The N_6 ring in the R-PN_6, stabilized through covalent bonding with dopant elements, was reported for the first time. Although R-PN_6 is a metastable phase, when the pressure increases to 100 GPa, R-PN_6 is located 66 meV/atom above the convex hull, indicating that this structure has the potential for synthesis at high temperatures and pressures.[5,15] The discovery of R-PN_6 provides new insights into the identification of N-rich compounds containing the N_6 ring.

At high pressures, the phonon dispersion curves of both the thermodynamically stable phase $C2/m$-PN_x (x = 6, 8, 10, 12, and 14) and metastable phase R-PN_6 show do not show imaginary frequencies; this result indicates their dynamical stability under high pressures (Fig. S4). When the pressure was reduced to 0 GPa, the six phases remained dynamically stable, indicating that they had the potential to be quenched to ambient pressure [Figs. 3(a)–3(c) and Fig. S5]. Furthermore, the elastic constant matrices of these six new phases under ambient conditions met the criteria for mechanical stability (Tables S1–S6). As indicated by the green-marked regions in Figs. 3(a)–3(c), with increasing N content, phonon softening occurred along the high-symmetry path A-Γ in $C2/m$-PN_x. Here, we refer to the phonon vibration mode with the lowest frequency at high-symmetry point A of $C2/m$-PN_x as Mode A. The frequencies of Mode A in $C2/m$-PN_x (x = 6, 8, 10, 12, 14, and 16) are shown in Fig. 3(d). As the N content increased, the frequency of Mode A decreased continuously. In $C2/m$-PN_{14}, the frequency of Mode A drops to 0.7 THz. This phonon frequency, which is close to zero, suggests that the system has reached its dynamic stability limit. When the N content was further increased to $C2/m$-PN_{16}, the frequency of Mode A became negative, leading to the instability of $C2/m$-PN_{16} and systems with higher N content (the structure and phonon dispersion curves are shown in Fig. S6).

To elucidate the mechanism behind phonon softening in the $C2/m$-PN_x system induced by the increase in N content, we conducted further studies on the phonon vibration modes. Figures 3(e) and 3(f) illustrate the vibrational Mode A in the $C2/m$-PN_6 and $C2/m$-PN_8, where the P-N octahedron, due to its greater mass, primarily governs the oscillations of the zigzag N-chain as a whole. Notably, the same phonon vibrational mode as Mode A was observed in the $C2/m$-PN_x systems (x = 6, 8, 10, 12, 14, and 16). As the N-chain lengthens, its mass increases, and the P-N octahedron becomes progressively less effective in restraining the zigzag N-chain, resulting in a reduction in the frequency of Mode A, which ultimately leads to the destabilization of the system. Therefore, in the $C2/m$-PN_x system, the length of the N-chain must be limit. The phonon dispersion curves of $C2/m$-PN_x demonstrate that

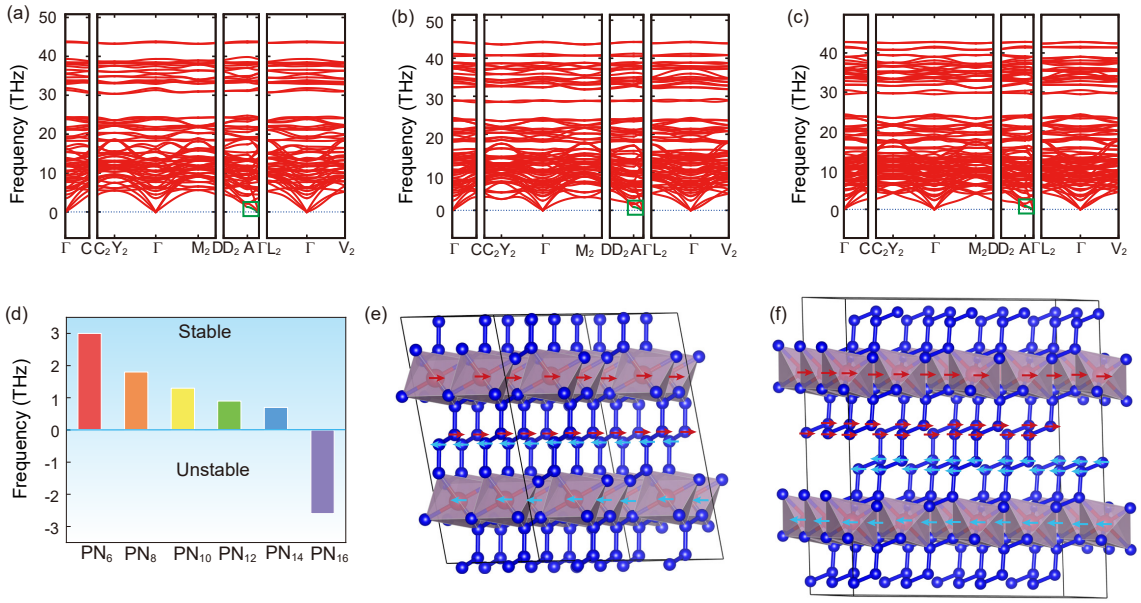

Fig. 3. Phonon properties of $C2/m$-PN_x. (a)–(c) show the phonon dispersion curves of $C2/m$-PN_{10}, $C2/m$-PN_{12}, and $C2/m$-PN_{14} at 0 GPa. The green-highlighted sections in the phonon dispersion curves indicate regions where phonon softening occurs as the length of N-chain increases. (d) Frequency of the lowest-frequency phonon vibration mode (Mode A) at the high-symmetry point A in the $C2/m$-PN_x (x = 6, 8, 10, 12, 14, and 16). (e) and (f) show Mode A in the $C2/m$-PN_6 and $C2/m$-PN_8. The direction of the arrow represents the direction of the vibration.

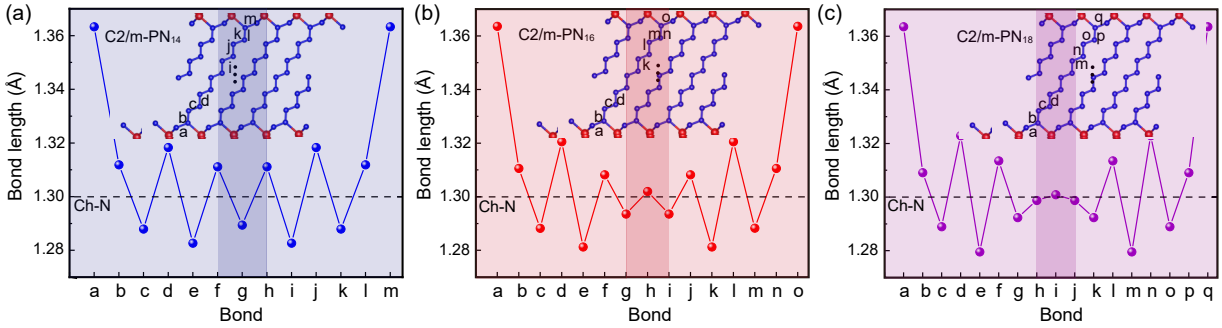

Fig. 4. N-N bond length of Ch-N and $C2/m$-PN_x (x = 14, 16, and 18) at 0 pressure. The letters on the x-axis in the figure represent different N-N bonds in $C2/m$-PN_x (x = 14, 16, and 18). (a)–(c) represent $C2/m$-PN_{14}, $C2/m$-PN_{16}, and $C2/m$-PN_{18}, respectively. The dashed lines represent the N-N bond lengths in the Ch-N structure. The dark areas in the figure represent the N-N bonds in the center of the N chains in the $C2/m$-PN_x system.

the longest zigzag N-chain capable of maintaining dynamic stability in the system consists of 14 N atoms [Figs. 3(a)–3(c), Fig. S5].

Figure 4 shows the variation in the N-N bond lengths in the N chains composed of different N atoms in the $C2/m$-PN_x system at 0 GPa. The dashed line indicates the N-N bond length of Ch-N. Evidently, each N-N bond in Ch-N has a length of 1.30 Å. Irrespective of the length of the zigzag N-chain in the $C2/m$-PN_x system, the N-N bond lengths at both ends of the zigzag N chains remain consistent because of their proximity to the P-N octahedra. Furthermore, the lengths of the N-N bonds oscillate from both ends toward the center, and the amplitude of the oscillation decreases as the bonds approach the center. In $C2/m$-PN_{14}, the length of P-N octahedra at both ends can significantly influence the entire N-chain because of the relatively short length of the N-chain. Consequently, the distribution of bond lengths in the zigzag N-chain of PN_{14} differs considerably from that in the zigzag N-chain of Ch-N [Fig. 4(a)]. As the length of N-chain increases, in PN_{16} and PN_{18}, the oscillation of N-N bonds around the central points of decreases, and the N-N bond lengths in the central region of the chain approach that of Ch-N (1.3 Å) [the darker areas in Figs. 4(b) and 4(c)]. In $C2/m$-PN_{18}, for instance, the bond length alternation vanishes for the two central N-N bonds (1.29 Å and 1.30 Å). This leads to instability of the $C2/m$-PN_{16} structure and other configurations containing longer zigzag N chains under ambient pressure, analogous to the behavior observed in the Ch-N structure (see Fig. S7). In summary, the alternating bond length variation of the N-N bonds is beneficial for the stability of the zigzag N chains.

Interestingly, in the PN_x system, no stable structure with an odd number of N atoms has been found. Therefore, in the PN_x system, structures with an even number of N atoms tend to be more energetically favorable than those with an odd number of N atoms. To investigate why the PN_x system is more energetically favorable when the

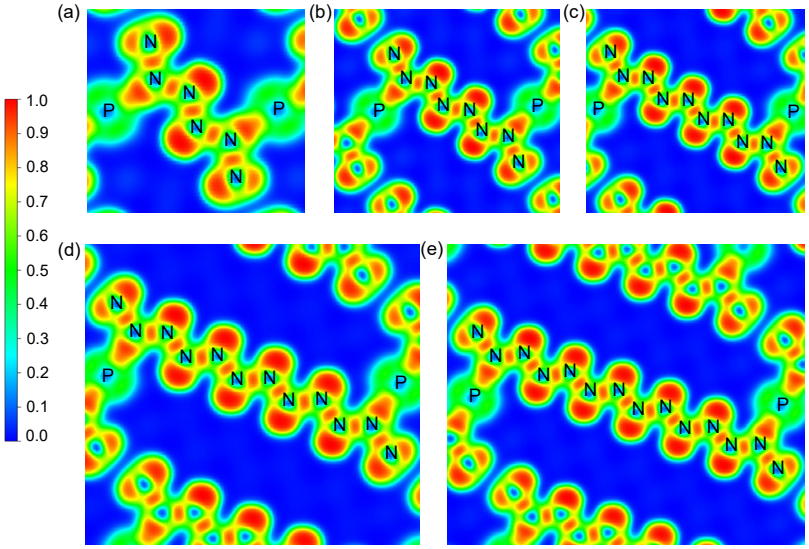

Fig. 5. ELF for $C2/m$-PN_x at 0 GPa. The ELF values on both sides of the N-chain are higher, with clear electron localization corresponding to the lone-pair electrons in the system. (a) $C2/m$-PN_6, (b) $C2/m$-PN_8, (c) $C2/m$-PN_{10}, (d) $C2/m$-PN_{12}, and (e) $C2/m$-PN_{14}.

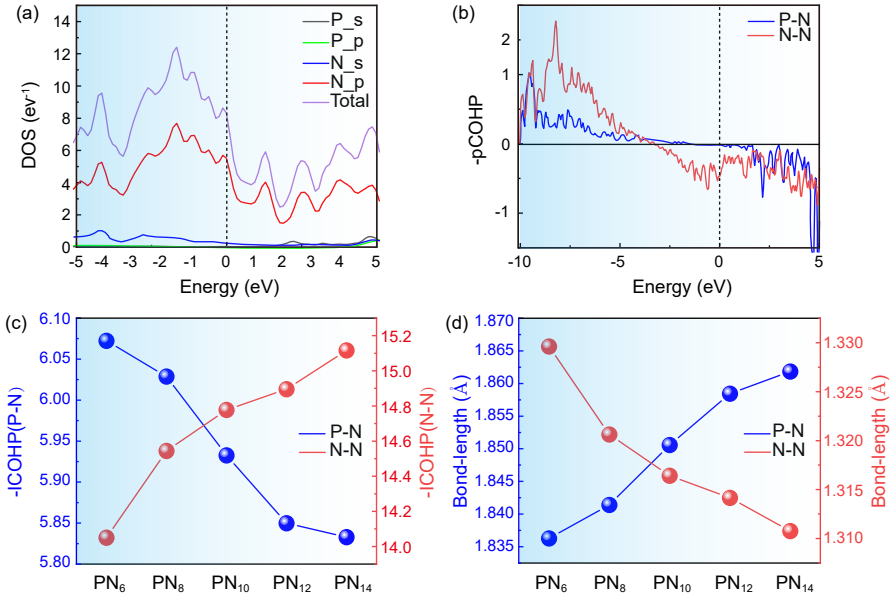

Fig. 6. (a) PDOS of $C2/m$-PN_{14} at 0 GPa, (b) pCOHP of P-N bonds and N-N bonds in $C2/m$-PN_{14} at 0 GPa, (c) ICOHP of P-N and N-N bonds in stable $C2/m$-PN_x at 0 GPa, (d) Average bond length of P-N and N-N bonds in stable $C2/m$-PN_x at 0 GPa.

number of N atoms is even, the electron localization function (ELF) for the energetically favorable phases $C2/m$-PN_x (x = 6, 8, 10, 12, and 14) were calculated. Figure 5 shows the existence of significant electron localization between the N atoms, indicating the formation of strong covalent bonds, which constitute the backbone of the zigzag chain. Moreover, the lone pair of electrons on both sides of the N-chain aligned linearly along the chain (the regions in Fig. 5, where the ELF value was close to 1), effectively maintained by the zigzag N-chain structure of $C2/m$-PN_x, which minimized the Coulomb repulsion of the system. According to valence shell electron pair repulsion theory,[67] a system with a smaller Coulomb repulsion implies better stability. When the number of N atoms is even, the lone-pair electrons on both sides of the zigzag chain are evenly distributed, minimizing the total Coulomb repulsion among them. For systems with an odd number of N atoms, the formation of equal amounts of lone-pair electrons on both sides of the zigzag N-chain is impossible; thus, the Coulomb repulsion in odd-numbered systems is higher than that in even-numbered systems. Consequently, in the P-N compounds, structures with an even number of N atoms tend to be more thermodynamically stable than those with an odd number of N atoms.

Figure 6(a) shows the electronic density of states (DOS) of $C2/m$-PN_{14} at 0 GPa. The DOS showed that the system did not exhibit a band gap, indicating that $C2/m$-PN_{14} displayed metallic properties. The DOS near

the Fermi level is mainly contributed by the N_2p electrons; thus the metallicity of the system primarily originates from the N_2p electrons. $C2/m$-PN_x (x = 6, 8, 10, and 12) also exhibit metallic characteristics (Fig. S8). The Bader charges (Fig. S9) indicated that in $C2/m$-PN_{14}, the P atoms transfer 2.8 electrons to the N atoms. These transferred electrons can effectively facilitate the polymerization of the N atoms.[68]

To further explore the bonding characteristics, we calculated the partial COHP (pCOHP) between P and neighboring N atoms in $C2/m$-PN_{14} at 0 GPa as well as between N atoms in the N-chain, as depicted in Fig. 6(b). Below the Fermi level, the P–N bonding states are fully occupied, whereas the P–N antibonding states above the Fermi level remain completely unoccupied, indicating the stability of the P-N bond. For the N-N bond, the bonding states were fully occupied, and some antibonding states were partially occupied. The calculated ICOHP values for the five stable phases are shown in Fig. 6(c). Although some antibonding orbitals of N are occupied, the ICOHP between N-N remains less than zero, indicating that the N-N bond is stable. As the N-chain grows, the strength of the P-N bonds gradually decreases, whereas the strength of the N-N bonds gradually increases. When the Nchain reached N_{10}, the strength of the N-N bond surpassed that of the P-N bond. To explain the change in the bond strength of the P-N and N-N bonds with Nchain length in $C2/m$-PN_x, the bond lengths of the P-N and N-N bonds in the system are shown in Fig. 6(d). Figure 6(d) shows that as the length of the N-chain increases, the average bond length of the P-N bond increases, whereas the average bond length of the N-N bond decreases. As a result, an increase in the N content causes the P-N bond length to increase and the N-N bond length to decrease, ultimately leading to a decrease in the strength of the P-N bond and an increase in the strength of the N-N bond. Furthermore, the bonding characteristics of these new P-N compounds are distinctly different from those of previously reported metal nitrides, such as BeN_2 and BaN_2.[69,70] Specifically, the pronounced electron localization observed between the P and N atoms (Fig. 5) indicated that the N chains were stabilized by covalent bonding. In contrast, in typical metal nitrides with chain-like nitrogen structures, no significant electron localization is observed between the metal atoms and nitrogen chains, which instead exhibit ionic bonding characteristics (Fig. S10).

Energy density (E_d), detonation velocity (V_d), and detonation pressure (P_d) are crucial parameters for assessing the HEDM performance. We calculated the energy density of PN_x compounds under ambient pressure using the dissociation pathway $6PN_x \rightarrow 2P_3N_5 + (3x-5)N_2$. α'-P_3N_5[71] and α-N_2[72] were chosen as the ground state phases. Subsequently, P_d and V_d were estimated using the Kamlet-Jacobs equations.[54] As depicted in Fig. 7, these five stable phases demonstrate significantly higher P_d, V_d, and volumetric energy densities (E_v) than traditional HEDMs such as TNT and HMX.[27,73] The metastable phase of R-PN_6 exhibits superior P_d, V_d, E_v, and E_d

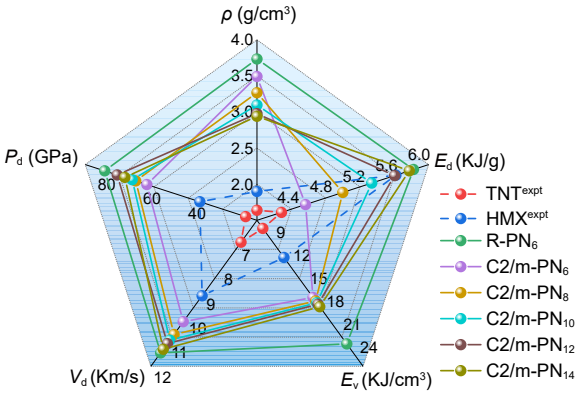

Fig. 7. Calculated energy density (E_d), volumetric energy density (E_v), detonation velocity (V_d), detonation pressure (P_d), and density (ρ) of P-N compounds.

compared to those of TNT, HMX, and the five stable phases. The E_d, E_v, V_d, and P_d values for R-PN_6 are 5.915 KJ/g, 22.087 KJ/cm^3, 11.447 km/s, and 81.415 GPa, respectively. The hardness values of $C2/m$-PN_x (x = 6, 8, 10, 12, and 14) and R-PN_6 are calculated. R-PN_6 exhibits a hardness of 47.59 GPa, which qualifies it as a superhard material. In addition to hardness, evaluating the anisotropy of the mechanical properties of materials is of great interest. Therefore, we calculated the spatial distribution of the Young's modulus (Fig. S11). The results show that $C2/m$-PN_x exhibits more pronounced anisotropy compared to R-PN_6.

Finally, given the promising application potential of $C2/m$-PN_x, viable synthetic routes must be discussed. Previous studies have shown that P and N_2 react under high pressures and temperatures to form P_3N_5, which contains PN_6 octahedra and is stable at a pressure of 0 GPa.[74] Notably, the PN_6 octahedron is a fundamental building block of $C2/m$-PN_x. Therefore, a synthesis scheme employing P_3N_5 and N_2 as precursors was proposed.

4. Conclusion. In this study, we realized zigzag polymeric N chains, similar to those found in Ch-N, within $C2/m$-PN_x (x = 6, 8, 10, 12, and 14), which can be quenched to ambient pressure and exhibit excellent detonation performance. Among them, the longest zigzag N-chain is found in $C2/m$-PN_{14}, which is composed of 14 N atoms. An analysis of the phonon properties of $C2/m$-PN_x (x = 6, 8, 10, 12, 14, 16, and 18) reveals that with an increase in the N-chain length, the P-N octahedra in the system struggle to maintain the stability of the zigzag N-chain, resulting in phonon softening and ultimately causing structural instability. Electronic structure analysis shows that zigzag N chains composed of an even number of N atoms form equal amounts of lone-pair electrons on both sides of the chain, effectively reducing the electron Coulomb repulsion. Consequently, the zigzag N chains with an even number of N atoms tended to be more energetically favorable. The metastable phase R-PN_6 contains an N_6 ring, which is stabilized for the first time by covalent bonds. Its high energy density (5.915 kJ/g), high Vickers hardness (47.59 GPa), and kinetic stability under

ambient pressure suggest its potential as a HEDM and superhard material. This study provides theoretical insights for the development of novel HEDMs.

Acknowledgments. This work was supported by the Anhui Provincial Natural Science Foundation (Grant No. 2508085J006) and CASHIPS Director's Fund (Grant No. YZJJ202207-CX). The calculations were partially performed at the Center for Computational Science of CASHIPS, ScGrid of the Supercomputing Center, Computer Network Information Center of the Chinese Academy of Sciences, and Hefei Advanced Computing Center.

References

[1] Liu R, Liu S, Zhang Y, Wang P, and Yao Z 2024 *Chin. Phys. Lett.* **41** 066301
[2] Shi X H, Liu B, Yao Z, and Liu B B 2020 *Chin. Phys. Lett.* **37** 047101
[3] Zhao L, Liu S, Chen Y, Yi W, Khodagholian D, Gu F, Kelson E, Zheng Y, Liu B, and Miao M S 2022 *Dalton Trans.* **51** 9369
[4] Liu S, Zhao L, Yao M, Miao M, and Liu B 2020 *Adv. Sci.* **7** 1902320
[5] Wang X, Wang Y, Miao M, Zhong X, Lv J, Cui T, Li J, Chen L, Pickard C J, and Ma Y 2012 *Phys. ReV. Lett.* **109** 175502
[6] Alemany M M G and Martins J L 2003 *Phys. Rev. B* **68** 024110
[7] Mattson W D, Sanchez-Portal D, Chiesa S, and Martin R M 2004 *Phys. ReV. Lett.* **93** 125501
[8] Martin R M and Needs R J 1986 *Phys. Rev. B* **34** 5082
[9] Zahariev F, Hu A, Hooper J, Zhang F, and Woo T 2005 *Phys. Rev. B* **72** 214108
[10] Wang X L, He Z, Ma Y M, Cui T, Liu Z M, Liu B B, Li J F, and Zou G T 2007 *J. Phys. Condens. Matter* **19** 425226
[11] Hooper J, Hu A, Zhang F, and Woo T K 2009 *Phys. Rev. B* **80** 104117
[12] Eremets M I, Gavriliuk A G, Trojan I A, Dzivenko D A, and Boehler R 2004 *Nat. Mater.* **3** 558
[13] Sun M, Yin Y, and Pang Z 2015 *Comput. Mater. Sci* **98** 399
[14] Tomasino D, Kim M, Smith J, and Yoo C S 2014 *Phys. Rev. Lett.* **113** 205502
[15] Laniel D, Geneste G, Weck G, Mezouar M, and Loubeyre P 2019 *Phys. Rev. Lett.* **122** 066001
[16] Laniel D, Winkler B, Fedotenko T, Pakhomova A, Chariton S, Milman V, Prakapenka V, Dubrovinsky L, and Dubrovinskaia N 2020 *Phys. Rev. Lett.* **124** 216001
[17] Benchafia E M, Yao Z, Yuan G, Chou T, Piao H, Wang X, and Iqbal Z 2017 *Nat. Commun.* **8** 930
[18] Xu Y X, Chen G, Du F, Li M, Wu L F, Yao D Y, Liu X D, Ding J F, Zeng Z, Liu R B, Lin H Q, and Wang X L 2024 *Sci. Adv.* **10** eadq5299
[19] Wu L, Xu Y, Chen G, Ding J, Li M, Zeng Z, and Wang X 2024 *Chin. Phys. B* **33** 126802
[20] Niu S, Xu D, Li H, Yao Z, Liu S, Zhai C, Hu K, Shi X, Wang P, and Liu B 2022 *Phys. Chem. Chem. Phys.* **24** 5738
[21] Peng F, Yao Y, Liu H, and Ma Y 2015 *J. Phys. Chem. Lett.* **6** 2363
[22] Prasad D L V K, Ashcroft N W, and Hoffmann R 2013 *J. Phys. Chem. C* **117** 20838
[23] Wang X, Li J, Xu N, Zhu H, Hu Z, and Chen L 2015 *Sci. Rep.* **5** 16677
[24] Yan M, Zhang S, Wang Y, and Ma F 2022 *Appl. Phys. Express* **16** 015505
[25] Shi X, Yao Z, and Liu B 2020 *J. Phys. Chem. C* **124** 4044
[26] Yuan J, Xia K, Ding C, Wang X, Lu Q, and Sun J 2022 *Matter Radiat. Extremes* **7** 038402
[27] Zhang J, Oganov A R, Li X, and Niu H 2017 *Phys. Rev. B* **95** 020103
[28] Ding C, Yuan J, Han Y, Zhang Z, Jia Q, Wang J, and Sun J 2023 *J. Chem. Phys.* **159** 184703
[29] Liu Z, Li D, Wei S, Liu Y, Tian F, Duan D, and Cui T 2019 *Phys. Lett. A* **383** 125859
[30] Liu S, Xu D, Liu R, Yao Z, and Wang P 2023 *Dalton Trans.* **52** 1000
[31] Li Y, Feng X, Liu H, Hao J, Redfern S A T, Lei W, Liu D, and Ma Y 2018 *Nat. Commun.* **9** 722
[32] Hou J, Weng X J, Oganov A R, Shao X, Gao G, Dong X, Wang H T, Tian Y, and Zhou X F 2021 *Phys. Rev. B* **103** L060102
[33] Steele B A and Oleynik I I 2017 *J. Phys. Chem. A* **121** 1808
[34] Jiao F, Zhang C, and Xie W 2021 *Phys. Chem. Chem. Phys.* **23** 7313
[35] Steele B A, Stavrou E, Crowhurst J C, Zaug J M, Prakapenka V B, and Oleynik I I 2016 *Chem. Mater.* **29** 735
[36] Laniel D, Weck G, Gaiffe G, Garbarino G, and Loubeyre P 2018 *J. Phys. Chem. Lett.* **9** 1600
[37] Zhao Z, Liu R, Guo L, Liu S, Sui M, Niu S, Liu B, Wang P, Yao Z, and Liu B 2022 *Inorg. Chem.* **61** 9012
[38] Bykov M, Bykova E, Chariton S, Prakapenka V B, Batyrev I G, Mahmood M F, and Goncharov A F 2021 *Dalton Trans.* **50** 7229
[39] Bykov M, Bykova E, Aprilis G, Glazyrin K, Koemets E, Chuvashova I, Kupenko I, McCammon C, Mezouar M, Prakapenka V, Liermann H P, Tasnadi F, Ponomareva A V, Abrikosov I A, Dubrovinskaia N, and Dubrovinsky L 2018 *Nat. Commun.* **9** 2756
[40] Bykov M, Fedotenko T, Chariton S, Laniel D, Glazyrin K, Hanfland M, Smith J S, Prakapenka V B, Mahmood M F, Goncharov A F, Ponomareva A V, Tasnadi F, Abrikosov A I, Bin Masood T, Hotz I, Rudenko A N, Katsnelson M I, Dubrovinskaia N, Dubrovinsky L, and Abrikosov I A 2021 *Phys. ReV. Lett.* **126** 175501
[41] Laniel D, Winkler B, Koemets E, Fedotenko T, Bykov M, Bykova E, Dubrovinsky L, and Dubrovinskaia N 2019 *Nat. Commun.* **10** 4515
[42] Zhang Y, Huang X, Yao Y, Zhang Z, Tian F, Chen W, Chen S, Jiang S, Duan D, and Cui T 2022 *Phys. Rev. B* **105** 125120
[43] Chen G, Zhang C, Zhu Y, Cao B, Zhang J, and Wang X 2025 *Matter Radiat. Extremes* **10** 015801
[44] Wang Y, Lv J, Zhu L, and Ma Y 2012 *Comput. Phys. Commun.* **183** 2063
[45] Kresse G and Furthmuller J 1996 *Phys. Rev. B* **54** 11169
[46] Kohn W and Sham L J 1965 *Phys. Rev.* **140** A1133
[47] Perdew J P and Wang Y 1992 *Phys. Rev. B* **45** 13244
[48] Perdew J P, Burke K, and Ernzerhof M 1997 *Phys. Rev. Lett.* **78** 1396
[49] Kresse G and Joubert D 1999 *Phys. Rev. B* **59** 1758
[50] Ahuja R 2003 *Phys. Stat. Sol. (b)* **235** 282
[51] Mills R L, Olinger B, and Cromer D T 1986 *J. Chem. Phys.* **84** 2837
[52] Togo A and Tanaka I 2015 *Scr. Mater.* **08** 1
[53] Grimme S 2006 *J. Comput. Chem.* **27** 1787
[54] Kamlet M J and Ablard J E 1968 *J. Chem. Phys.* **48** 36
[55] Deringer V L, Tchougréeff A L, and Dronskowski R 2011 *J. Phys. Chem. A* **115** 5461
[56] Sanville E, Kenny S D, Smith R, and Henkelman G 2007 *J. Comput. Chem.* **28** 899
[57] Tang W, Sanville E, and Henkelman G 2009 *J. Phys. Condens. Matter* **21** 084204

[58] Henkelman G, Arnaldsson A, and Jónsson H 2006 *Comput. Mater. Sci* **36** 354
[59] Yu M and Trinkle D R 2011 *J. Chem. Phys.* **134** 064111
[60] Wang V, Xu N, Liu J C, Tang G, and Geng W T 2021 *Comput. Phys. Commun.* **267** 108033
[61] Batyrev I G, Coleman S P, Ciezak-Jenkins J A, Stavrou E, and Zaug J M 2018 *MRS Adv.* **3** 499
[62] Raza Z, Errea I, Oganov A R, and Saitta A M 2014 *Sci. Rep.* **4** 5889
[63] Liu Y, Zhai C, Yao Z, and Liu B 2025 *J. Phys. Chem. Lett.* **16** 11876
[64] Yu S, Huang B, Zeng Q, Oganov A R, Zhang L, and Frapper G 2017 *J. Phys. Chem. C* **121** 11037
[65] Liu Z, Li D, Zhuang Q, Tian F, Duan D, Li F, and Cui T 2020 *Commun. Chem.* **3** 42
[66] Wei Q, Zhao C, Zhang M, Yan H, and Wei B 2019 *Phys. Lett. A* **383** 2429
[67] Gillespie R J and Nyholm R S 1957 *Q. Rev. Chem. Soc.* **11** 339
[68] Chen G, Niu C P, Xia W M, Zhang J, Zeng Z, and Wang X L 2023 *Chin. Phys. Lett.* **40** 086102
[69] Lin J, Zhu Z, Jiang Q, Guo S, Li J, Zhu H, and Wang X 2019 *AIP Adv.* **9** 055116
[70] Huang B and Frapper G 2018 *Chem. Mater.* **30** 7623
[71] Laniel D, Trybel F, Neri A, Yin Y, Aslandukov A, Fedotenko T, Khandarkhaeva S, Tasnadi F, Chariton S, Giacobbe C, Lawrence-Bright E, Hanfland M, Prakapenka V, Schnick W, Abrikosov I A, Dubrovinsky L, and Dubrovinskaia N 2022 *Chem. Eur. J.* **28** e202203123
[72] Wang B, Guégan F, and Frapper G 2022 *J. Mater. Chem. C* **10** 10374
[73] Stierstorfer J and Klapötke T M 2010 *Angew. Chem. Int. Ed.* **49** 6253
[74] Laniel D, Trybel F, Neri A, Yin Y, Aslandukov A, Fedotenko T, Khandarkhaeva S, Tasnadi F, Chariton S, Giacobbe C, Bright E L, Hanfland M, Prakapenka V, Schnick W, Abrikosov I A, Dubrovinsky L, and Dubrovinskaia N 2022 *Chemistry* **28** e202201998